Needle Probe Application for High-Resolution Assessment of Soil Spatial Variability in the Centrifuge

Zhihua Li[1], Bruce L. Kutter[2], Daniel W. Wilson[3]
Civil and Environmental Engineering
University of California, Davis, CA 95616

Kenneth Sprott[4]
Mechanical Engineering
California State University, Sacramento, CA 95819

Jong-Sub Lee[5] and J. Carlos Santamarina[6]
Civil and Environmental Engineering
Georgia Institute of Technology, Atlanta, GA 30332

1, 2 & 3, PhD candidate, Professor, and Research Engineer, Department of Civil & Environmental Engineering, University of California, Davis, CA 95616; Tel: (530) 752-7929; Fax: (530) 752-6758;
Email: blkutter@ucdavis.edu

4, Assistant Professor, Department of Mechanical Engineering, California State University, Sacramento, 6000 J St., Sacramento, CA 95819

5 & 6, Postdoctoral fellow and Professor, School of Civil and Environmental Engineering, Georgia Institute of Technology, Atlanta, GA 30332; Tel: (404) 894-7605; Fax: (404) 894-2278; Email: js245@mail.ce.gatech.edu

Abstract

This paper addresses the development of an electrical resistivity needle probe to be deployed during centrifuge model testing to assess with high-resolution the spatial variability of soil electrical resistivity. The probe is able to detect thin layers and accurately resolve interfaces between soil layers. While this paper focuses on its application to centrifuge models, the concept is equally useful for field applications.

The prototype probes are made from thin, stainless steel needles, with an insulated wire inserted into the needle, and bonded to it with epoxy resin, to form a coaxial probe (Cho et al. 2004). Different tip shapes including single-wedge, double-wedge and cone have been developed to optimize the spatial resolution of porosity, soil interfaces and layering.

The calibration and testing of the needle probe has been conducted both at Georgia Tech and UC Davis. This paper presents results of resistance versus depth and porosity versus depth, and compares the porosity based on measurement of mass and volume with the calculated porosity based on the needle probe measurements. Consequently, insertion effects are drawn and theoretical explanations are given.

For its deployment in the centrifuge, a special needle probe tool has been developed to be operated by the new NEES robot. Instrumentation, data acquisition and data processing issues associated with the needle probe robot tool are discussed. The basis for selection of materials, probe tip geometry, and the optimum frequency of AC electrical measurements is explained.

Keywords: needle probe, centrifuge, spatial variability, porosity, resolution, NEES, robot

Introduction

The porosity or void ratio is a fundamental property of a soil matrix. The porosity has a direct relationship to fundamental mechanical properties of soils such as dilatancy, peak friction angle and compressibility. The average porosity and the spatial variability of porosity are therefore considered to be valuable parameters to measure and to monitor in the field or in laboratory model tests.

To obtain high-resolution assessment of the porosity in centrifuge model tests, a miniature electrical needle probe has been developed to measure soil electrical resistivity. After normalizing the soil resistivity by the pore fluid resistivity, this information can be accurately correlated to the porosity of the soil (Archie 1942).

As part of the upgrades associated with a NEES (George E. Brown, Jr., Network for Earthquake Engineering Simulation) equipment development award, a new robot is being implemented on the UC Davis centrifuge. In addition to the needle probe tool, which is the focus of this paper, this robot will be able to access and interchange a variety of tools during flight: a stereo video camera tool, a cone penetrometer tool, an ultrasound tool and a gripper tool.

As an envisioned example, we may build a centrifuge model composed of layered sand of varying density. We would push the needle into the sand to determine the porosity distribution just after spinning up the centrifuge as a quality control test. Next, using the shaker mounted on the end of the centrifuge we may shake the model to induce liquefaction in some or all of the soil layers. After the shaking event, the needle probe may be used to profile the porosity distribution after the shaking event. Some layers of soil may densify and others may loosen due to shaking, liquefaction and the associated pore pressure re-distribution (Kulasingam et al. 2004). The needle probe will be able to determine which areas densify, and which areas loosen. The needle could also be used to investigate the spatial variability of porosity caused by simulated ground improvement in the model tests. Likewise,there is a strong potential for analogous applications of needle probe measurements in field applications.

Needle Probe Description

The needle probe is made from a thin, stainless steel needle, with an insulated wire inserted into the needle, bonded inside the needle with epoxy resin, to form a coaxial probe. The tip of the probe is grinded and polished to form a sharp edge. (Cho et al. 2004).

To optimize the spatial resolution of porosity, soil interface and layering, different tip shapes including double-wedge and cone have been tested. The following figure shows the photographs and schematic drawings of the double-wedge needle probe.

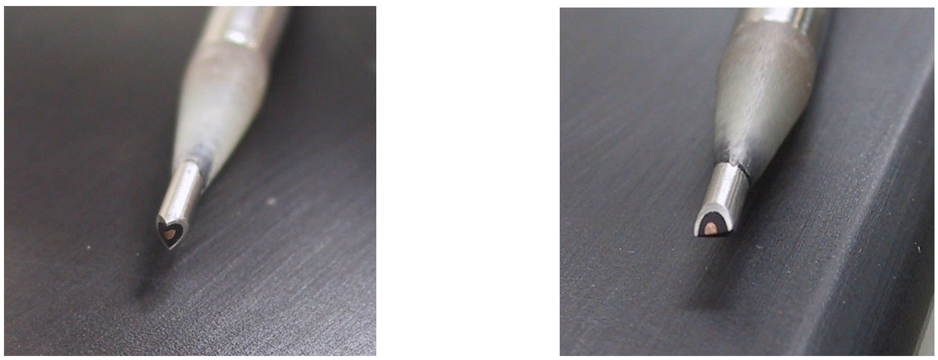

(a) Photographic images of the probe

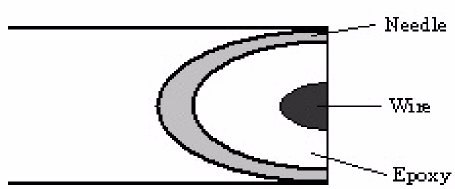

(b) Schematic view perpendicular to wedge tip

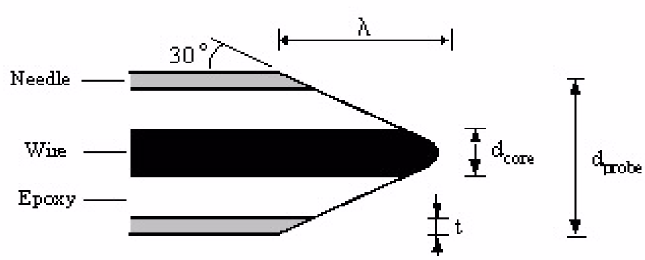

(c) Schematic view parallel to wedge tip

d_{probe} (mm)	t (mm)	d_{core} (mm)	λ (mm)
2.11	0.250	0.59	2.11

Figure 1. Double-wedge needle probe details: (a) photographic images of probe; (b, c) details of the probe tip.

Needle Probe Calibration in the Laboratory

Effect of instrumentation on electrical measurements. Figure 2 shows an equivalent circuit diagram of the needle probe and the tested soil. An HP-43192A Hewlett Packard low frequency analyzer was used to measure the complex impedance, Z^*_{meas}. The complex impedance ($Z^* = R + j \cdot X$) consists of the real part (the resistance, R) and an imaginary part (the reactance, X).

However, the desired information is the soil impedance, Z^*_{soil}. The measured impedance Z^*_{meas} is affected by the impedance of the probe, the cable, electrode polarization, and the soil itself. Stray values can be captured into series and parallel impedances Z^*_{ser} and Z^*_{par}.

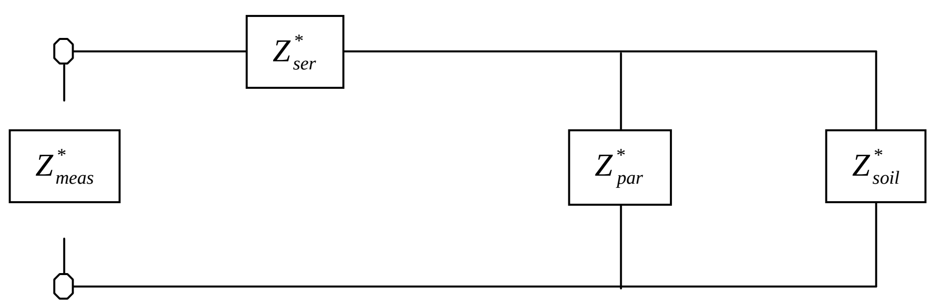

Figure 2. Equivalent circuit for the probe system.
Note: Asterisks denote complex quantity.

Calibration involves the determination of these parameters and their removal from the measured impedance to obtain the true impedance of the soil Z^*_{soil}. The impedances Z^*_{ser} and Z^*_{par} are obtained by two measurements. First the probe tip is shorted so that Z^*_{par} is effectively removed from the circuit; thus $\left(Z^*_{meas}\right)_{short} = Z^*_{ser}$. Second, the measurement is made with the tip in open air, which is assumed to have very large impedance compared to saturated soil, hence in this case $\left(Z^*_{meas}\right)_{open} = Z^*_{ser} + Z^*_{par}$.

These measurements allow the determination of the frequency dependent values, Z^*_{ser} and Z^*_{par}. The value of Z^*_{soil} may then be determined from Z^*_{meas} as

$$Z^*_{soil} = \left[\left(Z^*_{meas} - Z^*_{ser} \right)^{-1} - \left(Z^*_{par} \right)^{-1} \right]^{-1} \qquad \text{(at given frequency)} \tag{1}$$

The electrical response of a soil is modeled as a "lossy dielectric", which involves a resistor and a capacitor in parallel. Therefore, the impedance corresponding to the soil Z^*_{soil} is:

$$Z^*_{soil} = \left[\frac{1}{R_{soil}} + j\omega C_{soil} \right]^{-1} \tag{2}$$

where R_{soil} and C_{soil} are the resistance and the capacitance of the soil.

Correlation between resistivity and porosity. The formation factor, F is an index which has been shown experimentally to depend on the porosity, particle shape and size distribution and the direction of measurements (Archie 1942). Formation factor measurements have been used for determining volume changes during a pressuremeter test, for evaluating the in situ porosity of non-cohesive sediments, and for evaluation of in situ density and fabric of soil. The formation factor is defined as the ratio of the conductivity of the pore fluid, which saturates a particulate medium consisting of non-conductive particles, to the conductivity of the mixture of particles and pore fluid.

$$F = \rho_s / \rho_w \tag{3}$$

where ρ_w is the resistivity of the pore fluid and ρ_s is the resistivity of the soil.

On the basis of electromagnetic theory, Arulananadan and Sybico (1992) among others have presented analytical relations between the average formation factor, the porosity, n, and parameters associated with the shape and orientation of particles for anisotropic sands:

$$\bar{F} = n^{-\bar{f}} \tag{4}$$

where n is the porosity, $\bar{f}$ is the average form factor, and $\bar{F}$ is the average formation factor. Here, the average F refers to the arithmetic average of F measured in three orthogonal directions. The average form factor, $\bar{f}$, is a function of the particle shape and grain size distribution, and has been shown empirically and theoretically to be independent on the porosity. Hence, $\bar{f}$ can be measured from disturbed or reconstituted samples of the soil.

The anisotropy of the formation factor is quite small. Typically the horizontal and vertical formation factors are only different by about 5%. Furthermore, the needle probe produces electric field in all directions so we assume that the needle probe resistivitiy is representative of the average resistivity. The porosity can then be calculated using Eq. (5).

$$n = F_{needleprobe}^{\left(-1/\bar{f}\right)} \tag{5}$$

Given the geometry of the electrical field at the tip, the soil resistance R is related to the resistivity of the soil, ρ, by the shape factor S .

$$\frac{R}{\rho} = S \tag{6}$$

For infinite parallel plates, the shape factor is S = L/A where L is the distance between electrodes and A is the area of the electrodes. For the needle probe, the shape factor, S, may be determined empirically by measuring R in an aqueous electrolyte with a known conductivity. Alternatively, if there is free pore water above the ground surface, and if the pore fluid conductivity is uniform, the formation factor could also be determined more directly by

$$F = R_s / R_w \tag{7}$$

where R_s is the resistance of the soil measured by the needle probe and R_w is the resistance of the free pore fluid measured by the same needle probe. If there is no free pore fluid above the ground surface, R_w needs to be calculated from $R_w = S \cdot \rho_w$. ρ_w is the resistivity of the solution which may be determined by sampling the pore fluid and measuring with a conductivity meter.

Shape factor of the needle probe. To measure the shape factor of the needle probe, a series of Sodium Chloride (NaCl) solutions with different NaCl concentrations: 0.0001M, 0.0005M, 0.001M, 0.005M, 0.01M, 0.02M, 0.05M and 0.1M (M: Molality) were prepared as specimens.

The conductivities of the solutions were measured by the YSI 3200 conductivity meter (YSI Incorporated, Yellow Springs, Ohio). The needle probe is used to measure the impedances of the solutions. In the figure below shows the relationship of the needle probe resistance versus the resistivity of the solutions.

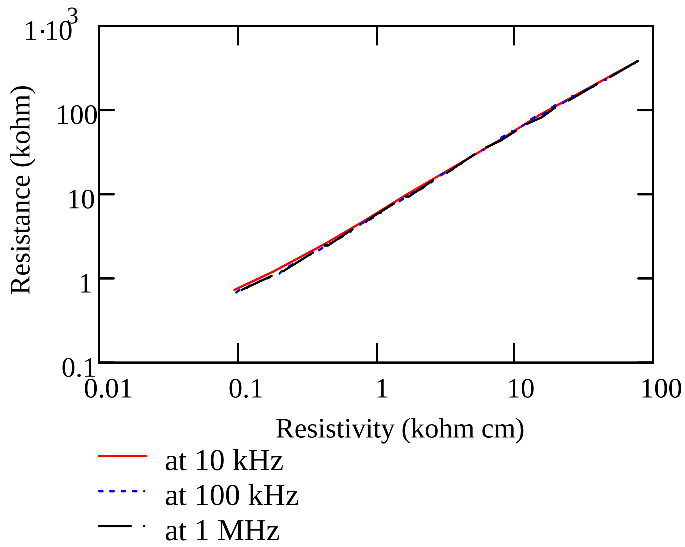

Figure 3. Needle probe resistance vs. resistivity of pure fluid at different frequencies.

The slope of the overlapping lines gives the shape factor S of the needle probe.

Operating Frequency. The optimal operating frequency is selected as 100 kHz based on considerations of corrosion, electrode polarization, and electrical resonance in the circuit. At lower frequency, electrode polarization causes increased contact resistance, reducing accuracy of measurements (Klein and Santamarina 1995). Results reported showed that corrosion of the electrodes is also more pronounced with high salinity water and is more significant at lower frequency. Figure 4 shows spectral data obtained with different ionic concentration electrolytes. Resistance R measurements exhibit the effects of electronic resonance at f>2 MHz and a relatively stable response below ~500 kHz. The resonant frequency depends on the needle size, cables, and soil–fluid conductivity. Because of low-frequency electrode effects and high-frequency resonance, resistance measurements can be most reliably performed between 10 and 1000 kHz.

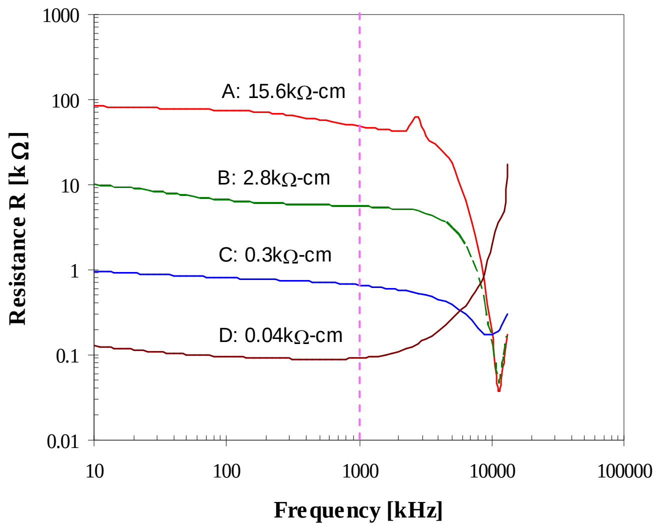

Figure 4. Resistance vs. frequency measured in NaCl solutions with different salt concentrations (A) 15.6, (B) 2.8, (C) 0.3, and (D) 0.04 kΩ cm (Cho et al. 2004).

Test Results

The needle probe lab testing has been conducted both at Georgia Tech and UC Davis. Test results in terms of resistance versus depth and porosity versus depth, and comparison between real porosity (based on measurement of mass and volume) and calculated porosity (based on the needle probe measurement) are presented and discussed next.

1. Interface detection: Loose-dense sand layers. A 100 mm diameter and 150 mm tall Plexiglas cylinder was used to enable placement of layered dry sand samples, evacuation and saturation with an electrolyte. A 30 mm thick layer of dense sand (prepared by vibration under a surcharge) was covered by a 35 mm thick layer of loose, dry pluviated sand (placed through a funnel with a small drop height). The cylinder was evacuated to -85 kPa and a de-aired 0.01M solution of NaCl in water was introduced from the bottom of the cylinder until a pool of water a few millimeters thick was formed on the top of the sand.

Then the needle probe was gradually inserted into the specimen and the impedance Z^*_{meas} was determined every 0.3 mm.

After correction from stray values, the resistance versus depth is plotted in Figure 5 (a). The formation factor is calculated and the relation between the formation factor versus depth is plotted in Figure 5 (b).

The corresponding porosity is calculated using Equation 4, where the form factor $\bar{f}$ for Nevada sand is taken as 1.31 (Sybico 1992).

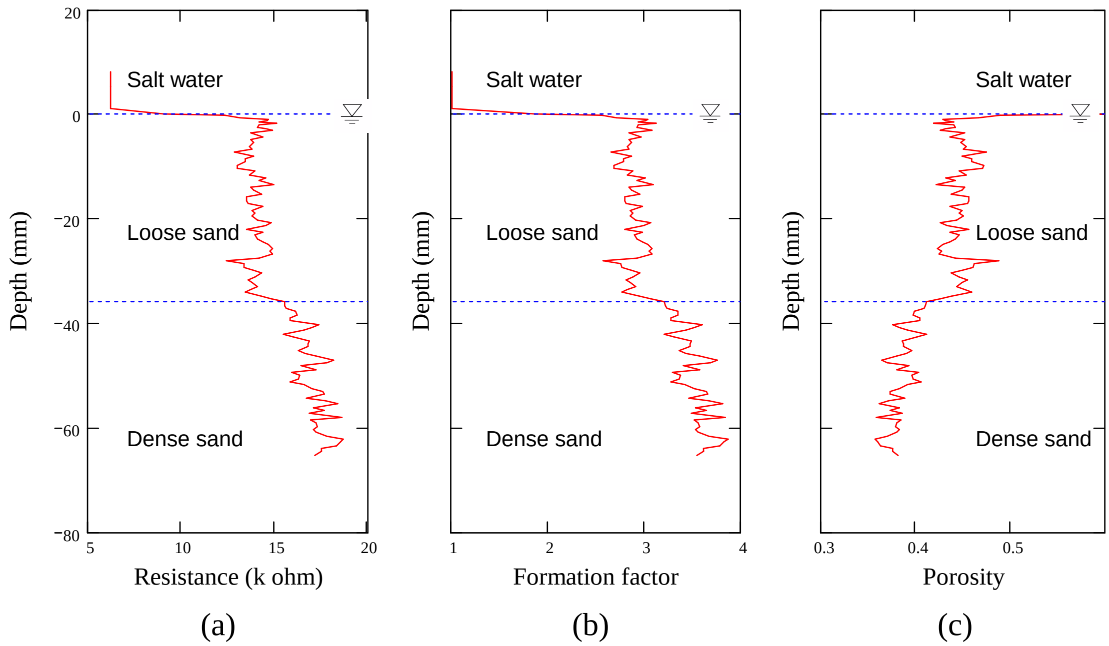

Figure 5. Spatial variability in a loose-dense layered sample saturated with 0.01M NaCl solution: (a) depth vs. resistance; (b) depth vs. formation factor; (c) depth vs. porosity.

The scatter observed in Figure 5 reflects real, small scale, variations in porosities (investigations, not presented here). From Figure 5, the length of the transition region at the dense-loose sand interface is obscured by the small-scale variations in porosity. Note that the air-water interface is detected with an accuracy of 2 mm or better. The resolution appears to be approximately equal to the distance between the stainless steel tube (external electrode) and the wire (core electrode) along the wedge.

The porosity calculated from the formation factor using the needle probe has been compared with the porosity calculated from direct mass and volume measurements for a series of tests. Figure 6 shows the relationship between these values.

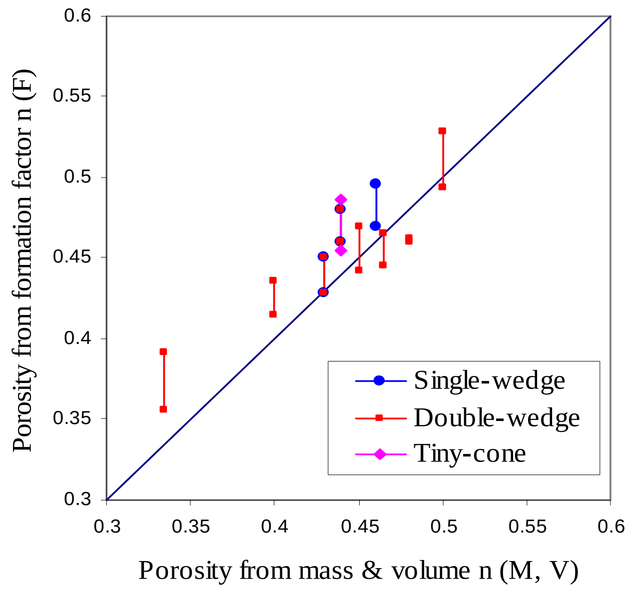

Figure 6. Relationship between the porosity calculated from the formation factor using the needle probe and the one calculated from mass and volume.

In Figure 6, the porosity calculated from formation factor is given as a range. That reflects the variability in the porosity versus depth curve (such as that shown in Figure 5) herein taken as the minimum and the maximum values. For the comparatively dense sands, in most cases the porosity calculated from formation factor using the needle probe is greater than the one calculated from mass and volume, while for the comparatively loose sands ($n \geq 0.4$), the porosity calculated from formation factor using the needle probe is close to the one calculated from mass and volume. This can be explained by critical state concepts: dense sands dilate and loose sands contract when they are sheared, in this case, due to the insertion of the needle probe.

Because the confining pressures are different in different tests (some tests were performed in a larger soil volume like in the centrifuge tests, some in smaller containers like in the cylinder tests), the critical void ratio, below which the sand dilates is expected to vary for different conditions.

2. Varved clay. This example shows the layer detection in varved clay using a double-wedge needle probe. After needle testing, the specimen is photographed and x-rayed. Images and resistance profiles are shown in Figure 7. The measured resistance profiles closely match the variability observed in the images.

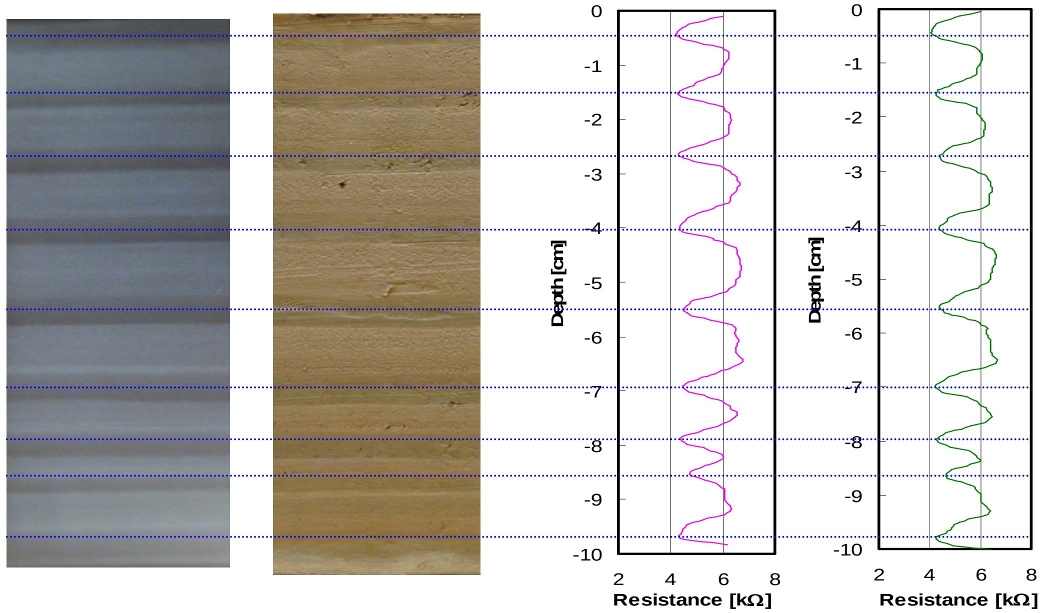

(a) X-ray (b) Photograph (c) Needle probe measurements

Figure 7. Detection of layering in varved clay: (a) X-ray image; (b) photograph; (c) needle probe measurements. The operating frequency is 100 kHz. (Cho et al. 2004).

Needle Probe Tool for the NEES Robot

The Center for Geotechnical Modeling at UC Davis operates a 9.1-m radius geotechnical centrifuge, which has the largest radius and largest platform area of any geotechnical centrifuge in the US. Figure 8 shows a picture of the centrifuge. This centrifuge is one of the equipment sites of the George E. Brown, Jr. Network for Earthquake Engineering Simulation (NEES). As part of the NEES project the centrifuge has been upgraded to increase the maximum centrifuge acceleration to 75 g, to install a biaxial shaker, advanced instrumentation, a robot and geophysical testing tools.

A gantry robot with changeable manipulator tools and an on-board tool rack can be used to perform multiple tasks without stopping the centrifuge. The robot can perform in-flight construction and inspection tasks and *in-situ* site characterization tests using a cone penetrometer and the needle probe.

The needle probe robot tool is composed of a 590-mm length and 6-mm diameter stainless steel tube, and the double-wedge needle probe attached to it through an insulating plastic (G-10) conical tip material glued to seal against the large tube and the double-wedge needle probe. The upper part of the G-10 connector is threaded into the large tube so that the attached needle probe can be readily replaced if needed, while the lower part is tapered into slope of 10º for smooth insertion of the tool into the soil. The needle probe is kept 5 mm short to prevent bending during the insertion under high confining pressures anticipated in the centrifuge tests.

Figure 8. Student working on model container on the geotechnical centrifuge at UC Davis.

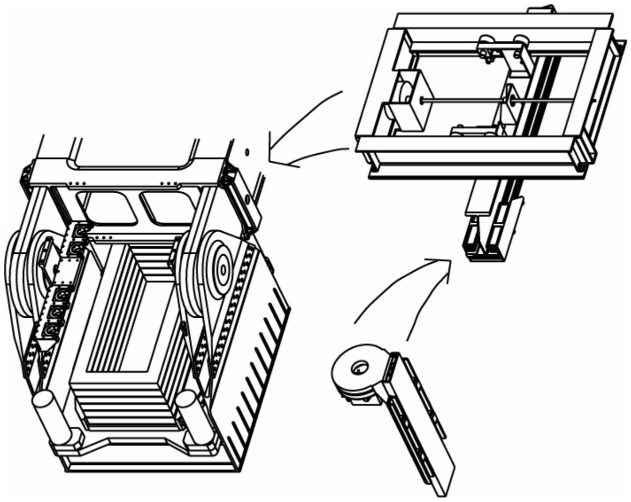

Figure 9. A 4 degree-of-freedom gantry robot has been added to the centrifuge. An onboard tool rack holds up to five tools for use.

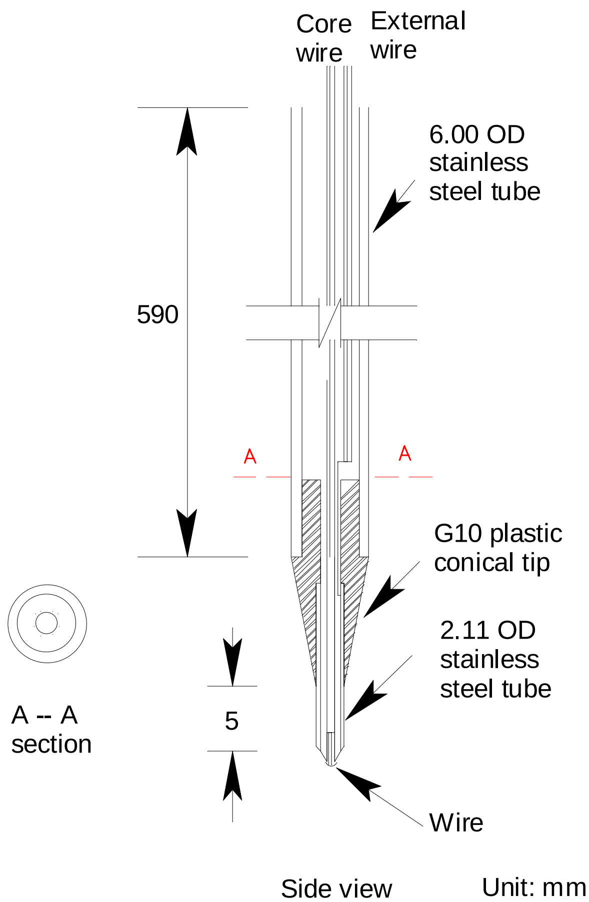

Figure 10. Details of needle probe tool for the NEES robot.

Two strain gauges are installed at the top of the large tube surface to detect x- and y-direction bending during needle probe insertion. Also, there is a load cell at the top of the tool to measure the load due to penetration of the needle probe.

From bottom to top, Figure 11 shows the long needle probe tool, two strain gauges attached, load cell above the needle probe tool to measure the loading, the interface between the needle probe tool and the robot, and the robot end effector. Figure 11(b) shows the clamping mechanism and electrical contacts between the tool interface and the robot end effector.

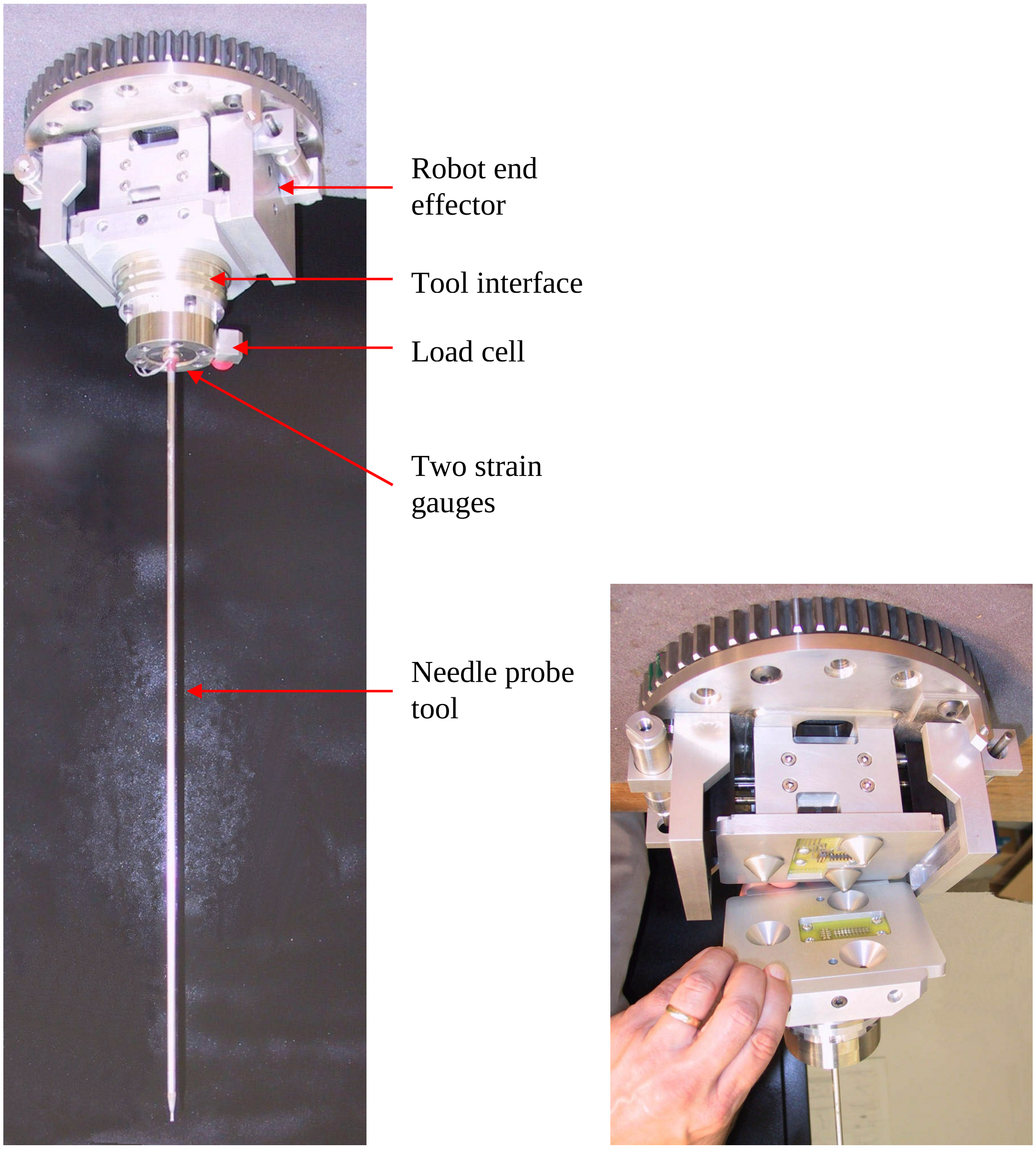

Figure 11. Needle probe tool: (a) needle probe tool clamped by robot end effector; (b) details of the electrical contact interface, alignment cones and tool clamping mechanism.

Instrumentation, Data Acquisition and Data Processing

The basic idea is to send out voltage signals from a digital to analog converter using a high speed data acquisition card to a series circuit composed of the needle probe and a known value resistor. The resistance is determined by measuring the voltage across the probe electrodes, and by measuring the voltage across the resistor to compute the current passing through the needle probe electrodes.

The typical resistance of the needle probe in sand saturated with 0.01 M NaCl electrolyte, is in the range of 2~20 kΩ. Thus, a resistor of 10 kΩ is chosen for the series resistor in the circuit. After carefully considering the demands for the signal generator including voltage and current capacity, sampling rate, input & output resolution, the number of D/A & A/D channels, and frequency, a National Instruments PCI-6115, 10MS/s, 12-bit, 4 analog input simultaneous-sampling multifunctional DAQ is chosen to be the D/A signal generator and the A/D converter. The wiring diagram is shown in Figure 13.

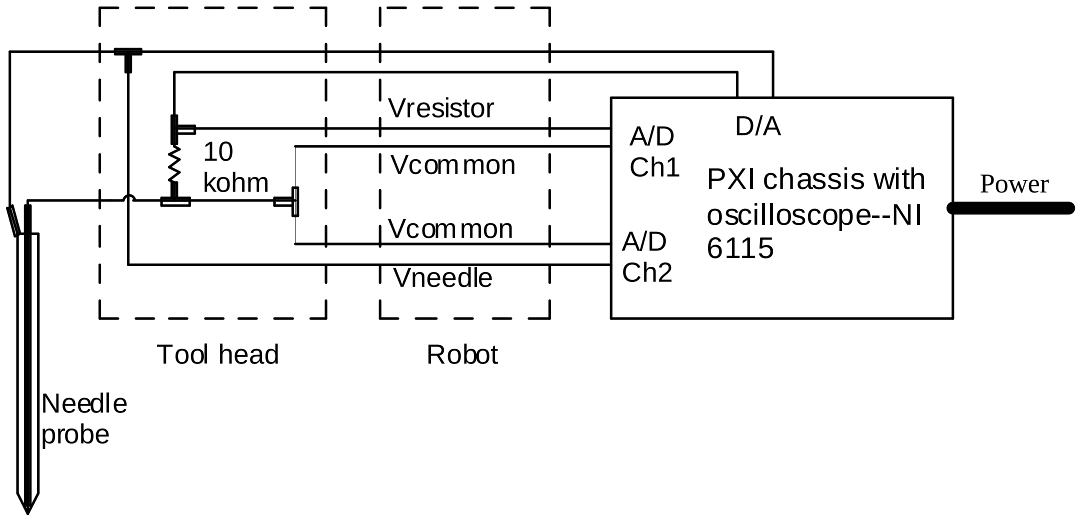

Figure 13. Needle probe wiring and connection to data acquisition board.

A LabVIEW program has been compiled to interpret the data. It is composed of the output part (D/A) and the input part (A/D). In the D/A output part, a digital sinusoidal excitation is applied to the circuit. The signal type, operating frequency, phase, amplitude, offset and timing, can be adjusted through the software. Based on considerations described above (corrosion, electrode polarization, and electrical resonance in the circuit), we have selected 100 kHz as an optimal value for this measurement.

In the A/D input part, the voltage outputs across the resistor and the needle probe are detected in forms of amplitude, phase and frequency using LabVIEW sub-VI (Visual Instruments): Extract Single Tone Information. Current flowing through the circuit is calculated as the voltage drop across the resistor divided by its resistance. The amplitude and the phase of the impedance measured by the needle probe are calculated based on the measured voltage across the needle probe and the current flowing through it. Figure 14 shows an example of the measured signals. The frequency used is 1.024 kHz for demonstration.

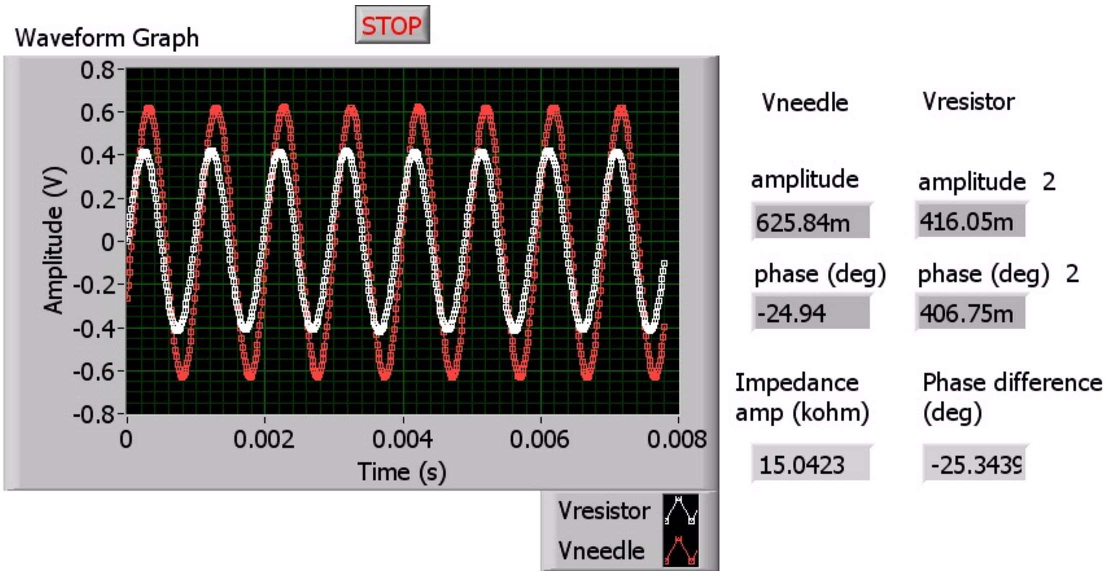

Figure 14. An example of the measurement results in LabVIEW front panel.

In this example, the voltage amplitude output from the signal generator is +/- 1V. The measured voltage amplitudes across the resistor and the needle probe are 0.416 V and 0.626 V, respectively. So the amplitude of the measured impedance is about 15 kΩ. The phase angle is the difference between the two measured phases which is about 25º. To precisely calculate the resistance and capacitance of the soil, the equivalent circuit correction discussed earlier is applied.

Conclusions

This paper addresses the development of an electrical resistivity needle probe for the centrifuge model testing to assess the spatial variability of soil porosity with high-resolution. The basis for selection of materials, probe tip geometry, and the optimum frequency of AC electrical measurements is explained. Instrumentation, data acquisition and data processing issues associated with the needle probe robot tool are discussed. While this paper focuses on application to centrifuge models, the concept is equally useful for field applications.

Experimental results show that the probe has great potential to accurately resolve interfaces between soil layers and small local variations in void ratio. The needle probe insertion effect in the measured porosity is in agreement with critical state predictions. The resolution of the needle probe is approximately equal to the spacing between the electrodes in the probe along the wedge.

References

Archie, G. E. (1942). “The electrical resistivity log as an aid in determining some reservoir characteristics.” *A.I.M.E. Trans*, 146, 54-61.

Cho, G. C., Lee, J. S., and Santamarina, J. C. (2004). “Spatial Variability in Soils: High Resolution Assessment with Electrical Needle Probe.” *J. Geotech. Engrg.*, ASCE, 130(8).

Klein, K., and Santamarina, J. C. (1995). “Polarization and conduction of clay-water-electrolyte systems.” *J. Geotech. Eng.*, 121(3), 243–248.

Kulasingam, R., Malvick, E. J., Boulanger, R. W., and Kutter, B. L. (2001). “Void redistribution and localization of shear strains in model sand slopes with silt seams: Report on first year activities.” Univ. of Calif., Davis, Calif.

Kutter, B. L., Arulanandan, K., and Dafalias, Y. F. (1979). “A Comparison of Electrical and Penetration Methods of Site Investigation.” *Offshore Technology Conference*, Houston, TX, 1105-1115.

Lide, D. R. (2003). *Handbook of Chemistry and Physics (84th Edition)*, CRC, Boca Raton, FL, **5**-94.

Kulasingam, R., Malvick, E. J., Boulanger, R. W., Kutter, B. L. (2004). “Strength Loss and Localization at Silt Interlayers in Slopes of Liquefied Sand.” *J. Geotech. Engrg.*, ASCE, November 2004.

Santamarina, J. C. in collaboration with Klein, K. A., and Fam, M. A. (2001). *Soils and waves—Particulate materials behavior, characterization and process monitoring*, Wiley, New York.

Sybico Jr., J. A. (1992). *Post-liquefaction settlement of sands,* MSc Thesis, Univ. of Calif., Davis, Calif.

Acknowledgement

This study is supported under the Network for Earthquake Engineering Simulation (NEES) program of the National Science Foundation under award number CMS-0086566. Any opinions, findings, and conclusions or recommendations expressed in this study are those of the author(s) and do not necessarily reflect the views of the National Science Foundation.

Development technicians Daret Kehlet and Tom Coker in Dept. of Civil and Environ. Engr. helped to make the needle probes and testing circuits.